Gold Electroless Reduction in Nanosized Channels of Thiol-Modified SBA-15 Material

Nikolay Petkov,* Norbert Stock, and Thomas Bein

Department of Chemistry, University of Munich, Butenandtstrasse 5-13 (E), 81377 Munich, Germany

Received: January 25, 2005; In Final Form: April 1, 2005

A new procedure for the preparation of high aspect ratio Au nanowires utilizing gold electroless reduction in the hexagonally ordered, thiol-modified nanosized channels of the SBA-15 material is reported. Two different Au precursors were adsorbed onto pedant thiol groups, covalently bonded to the mesoporous silica surface, and used as seeds to grow extended Au nanostructures by treatment in Au electroless reduction bath. It is shown that the dimensions and the assembly of the Au seeds are important parameters for the subsequent electroless reduction process. The $[AuCl_4]^-$ ions complexed to the TOAB molecules assembled on the thiol-modified mesoporous surface of the SBA-15 material are suitable precursors for the subsequent gold electroless reduction. The resulting structures are several micrometer long Au nanowires with uniform diameters of about 5 nm, having large single-crystalline domains. The TEM results clearly show that the growth of the Au nanowires is templated by the channel structure of the SBA-15 material.

1. Introduction

Nobel-metal nanostructures prepared by bottom-up approaches as one-dimensional nanowires or arrays of ordered nanosized particles are considered to be key elements for the development of future nanotechnology.[1−3] Among these, considerable attention has been paid to the Au nanostructures because of their appealing electrical properties that are essential when the preparation of interconnections and functional units for electronic, optoelectronic, electrochemical, and electromechanical devices is required.[4,5] The preparation of noble-metal nanostructures by applying templating methods within the confined spaces of host materials, such as anodic alumina, carbon nanotubes, or mesoporous solids, is an attractive opportunity.[6−11]

Metal infiltration through wet impregnation and metal-organic chemical vapor deposition in the hollow channels of different porous supports are popular techniques used to load them with metallic particles for different catalytic applications.[12,13] These approaches have been expanded to the preparation of continuous metal nanostructures.[11,14,15] Au nanostructures, nanowires, or nanoarrays can be prepared in mesoporous hosts by applying a direct wet impregnation technique with $H[AuCl_4]$, or in situ by complexation of the Au precursors on the organically modified mesoporous surface.[11,16−19] Recently, one-pot synthesis of ordered mesoporous material loaded with Au nanoparticles was reported where the $H[AuCl_4]$ was directly added to the initial synthesis sols.[20]

A prerequisite for the successful impregnation of the silica-based mesoporous solids with the $H[AuCl_4]$ is the adjustment of the isoelectric point of the host matrix so that the anionic $Au(OH)_xCl_{4-x}$ complexes are coordinated onto the mesoporous surface. For example, at pH 6−10 where the usual wet impregnation is done, the mesoporous silica surface is negatively charged (the isoelectric point of silica is around 2) and no coordination of the Au precursors is expected. A useful strategy is to modify the mesoporous surface with cationic functional groups that will enhance the interaction between the anionic Au complexes and the silica surface.[16,18] On the other hand, thiol-functionalized mesoporous surfaces were used to directly assemble Au nanostructures by size-selective extraction of the Au nanoparticles from nanosized colloidal Au suspensions.[21]

An important factor that influences the synthesis of the Au nanostructures in the host matrixes is the choice of the reducing agent. Usually the $H[AuCl_4]$ precursor is reduced in a hydrogen flow at elevated temperatures[11,14,16] or by using chemical reducing agents, such as $NaBH_4$ or citrate, to obtain metallic Au nanostructures.[18,19] When high-temperature hydrogen reduction is used the mobility of the Au species is high enough to form bigger clusters on the outer surface of the host matrix.[11] To overcome this problem mild chemical reduction conditions were suggested that make the final size of the Au nanostructures only dependent on the pore size of the host matrix.[18] Another promising approach to obtain continuous metal nanowires is metal electroless reduction.[22] The electroless reduction methods use metal ions or catalyst nanoparticles to nucleate and guide the growth of continuous metal nanostructures. It has been shown that chiral lipid tubules can be metallized by electroless reduction giving nanometer thin metal wires.[23] Metallized DNA molecules were also subjected to electroless reduction, resulting in metal nanowires between two metal electrodes.[24,25]

Here we report a three-step procedure for the preparation of Au nanowires in the hexagonally ordered, nanosized channels of the SBA-15 host (see Scheme 1). First, the SBA-15 mesoporous surface was modified with thiol functionalities followed by assembly of Au precursors that were used as seeds for subsequent electroless reduction in a gold plating bath. Two different methods for the assembly of the catalytically active Au precursors were explored: (i) direct assembly of 5−6 nm Au particles prepared in tetraoctylammonium bromide (TOAB) and (ii) Au precursors containing $[AuCl_4]^-$ ions complexed to TOAB molecules. Because of the extremely thiophilic nature of Au, the Au precursors can chemisorb onto the polymeric adhesive layers having pedant thiol groups and covalently bonded to the mesoporous silica surface. These surface-confined Au precursors were then used as seeds to grow extended Au

* To whom correspondence should be addressed. E-mail: nikolay.petkov@cup.uni-muenchen.de.

10.1021/jp050429i CCC: $30.25
Published on Web 04/30/2005

SCHEME 1: Schematic Representation of the Synthetic Steps To Obtain Au Nanostructures in the SBA-15 Material

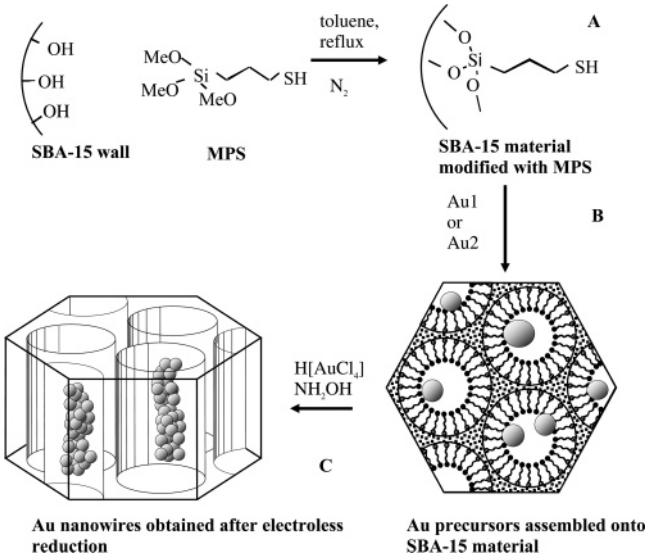

nanostructures by treatment in a gold electroless reduction bath. To our knowledge the obtained Au nanostructures are the first examples of high aspect ratio Au nanowires prepared by gold electroless reduction and confined in the nanosized channels of the SBA-15 material.

2. Experimental Section

2.1. Synthesis of SBA-15 Material and Grafting of Thiol Functionalities. The mesoporous SBA-15 material was prepared according to methods described in the literature resulting in microscopic SBA-15 rods.[26] In a typical synthesis, 2.0 g of Pluronic123, triblock copolymer (BASF) were dissolved under stirring in 30.0 g of 4 M HCl and 45.0 g of water, followed by addition of 3.1 g of tetramethoxysilane (TMOS, Aldrich). This mixture was homogenized and stirred at 40°C for 20 h and then kept at 100 °C for an additional 24 h without stirring. The final molar ratio of the synthesis gel is 1TMOS:0.017Pluronic123:6HCl:125H_2O. The final product was recovered by filtration and dried at room temperature without washing. Template-free SBA-15 material was obtained by calcination at 500 °C for 6 h. Calcined SBA-15 solid was modified with thiol groups. A sample of 50 mg of the mesoporous silica SBA-15 material was dehydrated at 120 °C in a vacuum, and then stirred in 30 mL of dry toluene (Fluka) containing 5 mL of 3-mercaptopropyltrimethoxysilane (MPS, Fluka) (Scheme 1, A) under refluxing conditions applying standard Schlenk-line techniques for 20 h.

2.2. Preparation of the Au Precursors. Two types of Au precursors were prepared in this study that are referred to as Au1 and Au2 precursors. Special attention was paid that clean glassware (aqua-regia) is used in all synthesis.

Au1 colloidal gold was synthesized according to literature methods and is expected to give 4−5 nm Au nanoparticles.[27] A 1.5-mL sample of a 30 mM aqueous solution of hydrogen tetrachloroaurate $H[AuCl_4]0{\cdot}3H_2O$ (Aldrich) was mixed with 4 mL of a 50 mM solution of TOAB (Aldrich) in toluene and shaken vigorously in a separation funnel. After quantitative transfer of the tetrachloroaurate to the organic phase, 1.75 mL of freshly prepared 0.5 M sodium borhydride $NaBH_4$ (Aldrich) was added at once under stirring and reacted for 15 min. Finally, the ruby-colored organic phase was separated carefully, washed once with 0.1 M sulfuric acid to remove access of borhydride, and used for further studies.

Au2 solution was prepared similar to Au1 but the $NaBH_4$ reduction step was omitted. The final orange-brown toluene solution was further used to directly assemble the Au precursors in the thiol-modified mesoporous hosts.

2.3. Assembly of the Au Precursors and Gold Electroless Reduction. Usually, a sample of 40 mg of MPS-modified SBA-15 material (SBA-15-MPS) were stirred for 20 h at room temperature with 5 mL of the Au1 colloid or Au2 solution (Scheme 1, B). After the assembly of the Au precursors the powder was collected by filtration, washed with excess amounts of solvent, and dried at 60 °C for at least 24 h.

The last step of the synthetic procedure involves electroless reduction (see Scheme 1, C). A sample of 30 mg of SBA-15 material modified with the Au1 or Au2 precursors was immersed in a gold electroless reduction bath[28] consisting of 3 mLof 4 mM $NH_2OH{\cdot}HCl$ and 3 mL of 30 mM $H[AuCl_4]0{\cdot}3H_2O$ for 20 min. After the electroless reduction the powder was collected by filtration, washed with excess amounts of solvent, and dried at 60 °C for at least 24 h. The samples described above are listed in Table 1.

2.4. Characterization. The mesophase structure of the host materials and the samples loaded with Au nanostructures were confirmed by X-ray diffraction (Scintag XDS 2000, Cu Kα radiation). N_2 adsorption−desorption isotherms were recorded on a NOVA 4000e Surface Area & Pore Size Analyser after evacuation of the samples at 120 °C. The functionalization process of the SBA-15 material was followed by FT-Raman and solid-state NMR spectroscopy. The FT-Raman spectra were recorded with a Bruker Equinox 55-106v/S spectrometer equipped with a Raman module (9395 cm^{-1} laser, 4 cm^{-1} resolution, 80 mW laser power, 2000 scans). Proton-decoupled ^{13}C and ^{29}Si solid-state NMR spectra were recorded on a Bruker DSX Avance spectrometer. The loading of the host support with organic functionality was followed by thermogravimetric analysis (TGA; Du Pont 951, Thermal Analyzer). The elemental composition and the surface morphology of the powder samples were determined with a SEM (JEOL, JSM 65007, field emission SEM equipped with Oxford EDX detector). TEM measurements were performed with a JEOL JEM 2010 transmission electron microscope operating at 200 kV.

3. Results and Discussion

3.1. Thiol Functionalization of the SBA-15 Material. The XRD patterns of the calcined and MPS-modified SBA-15 samples show that the mesophase structure is preserved after the thiol functionalization. The patterns correspond to (*p*6*m*) hexagonal mesophase structure with intense first-order (100) reflection and less intensive second-order (110) and (200) reflections (Figure 1).[11] After postsynthesis modification, the intensity of all reflections decreases suggesting diminished mesostructural order and/or reduced scattering contrast between the silica wall and the porous system.[16]

The N_2-adsorption isotherms of the calcined and MPS-modified samples are shown in Figure 2. Typical type IV N_2-adsorption isotherms with distinct hysteresis loops and steep adsorption/desorption steps were recorded that indicate a narrow pore size distribution. Most importantly, after the postsynthesis silylation the shape of the isotherms is preserved; no pore blocking or mesophase distortion is observed. The specific surface area (S_{BET}), the total pore volume (V_t), and the mean pore size calculated from the BJH model (D_{BJH}) show decreased values for silane-grafted samples in comparison to the parent SBA-15 material in correspondence to the pore-filling effect (Table 1).[18,29,30]

TABLE 1: N_2-Adsorption Data and Au Particle Size for the Au Nanostructures in SBA-15 Material

sample	manipulation	S_{BET} ($m^2\ g^{-1}$)[a]	V_t ($cm^3\ g^{-1}$)[b]	D_{BJH} (nm)[c]	size of Au (nm)[d]	size of Au (nm)[e]
SBA-15-calc	calcined SBA-15	887	1.17	5.4		
SBA-15-MPS	MPS-modified SBA-15	468	0.62	5.3		
SBA-15-MPS-Au1	assembly of Au1	266	0.42	4.4	spheres: 5−7 nm	5.7
SBA-15-MPS-Au1-red	electroless reduction	168	0.27	4.1	spheres: 20−70 nm	20.8
SBA-15-MPS-Au2	assembly of Au2	328	0.48	4.5		
SBA-15-MPS-Au2-red	electroless reduction	191	0.32	4.2	wires: 5 nm thick, several microns long	22.7

[a] The surface area S_{BET} is calculated from the BET model. [b] The total volume adsorbed, V_t, is calculated form single point measurement at $P/P_o = 0.994$. [c] The pore size distribution, D_{BJH}, is determined by the BJH model applied to the desorption branch of the isotherm. [d] The Au particle size is determined by the TEM measurements. [e] The Au crystalline size is determined from the Scherrer equation.

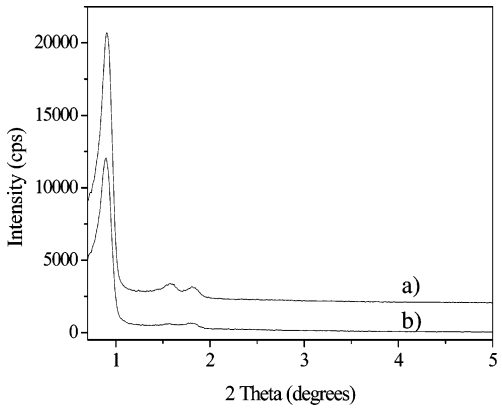

Figure 1. XRD patterns of the (a) calcined and (b) thiol-modified SBA-15 materials.

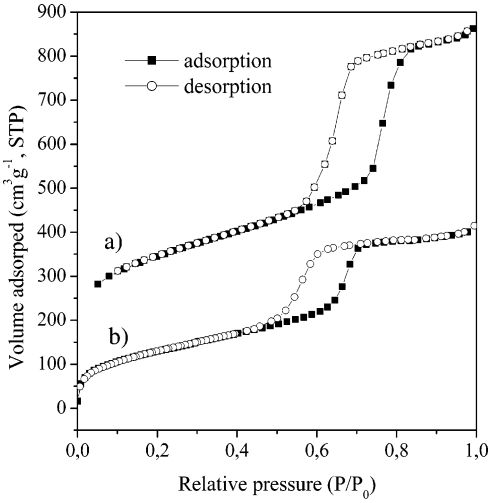

Figure 2. N_2-adsorption isotherms of the (a) calcined and (b) thiol-modified SBA-15 materials (the isotherms are offset with 200 $cm^3\ g^{-1}$).

Thermal analysis was used to evaluate the loading degree with a molecular functionality. The SBA-15-MPS sample shows a weight loss of 7 wt % (or about 14 wt % loading with MPS, assuming that the weight loss is only due to the combustion of the organic part of the silane and that siloxane bonds are formed) that corresponds to about 0.63 mmol/g of SiO_2 or 0.45 MPS molecule per nm^2 of the mesoporous surface. A fully dense monolayer of MPS molecules on the MCM-41 surface ($S_{BET} \sim$ 900 m^2/g) has been evaluated to be 5 molecules per nm^2.[29] Assuming full coverage with MPS molecules (with the length of the MPS molecule of about 0.42 nm, calculated from geometrical considerations) of the cylindrical mesopores with average diameter of 5.4 nm and specific surface area of 887 $m^2\ g^{-1}$ of the calcined SBA-15 sample, the total decrease of the mesoporous volume is estimated to be about 0.68 $cm^3\ g^{-1}$.

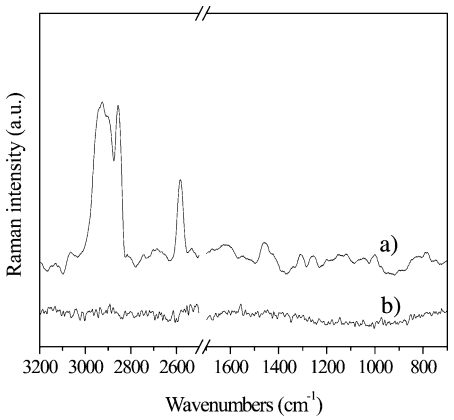

Figure 3. FT-Raman spectra of the (a) calcined and (b) thiol-modified SBA-15 materials.

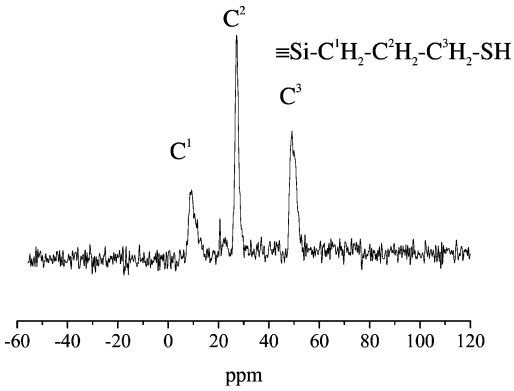

Figure 4. ^{13}C NMR spectra of the thiol-modified SBA-15 material.

This is more than the decrease of the total pore volume (V_t) measured by the N_2 adsorption (0.55 $cm^3\ g^{-1}$) and suggests sparsely covered mesoporous surface with MPS molecules. These results are in accordance with the ^{29}Si NMR data shown below.

Additional evidence for the silane modification of the mesoporous surface is obtained by FT-Raman and solid-state ^{13}C and ^{29}Si NMR spectroscopy. Figure 3 shows the Raman spectra of the SBA-15-calc and SBA-15-MPS samples. As expected, the spectrum of the SBA-15-calc does not show any Raman peaks in the examined region in correspondence with the full template removal during the calcination process. In the high-frequency region, the bands that are typical for the $-CH_2-$ asymmetric- and symmetric-stretching vibrations are seen in the spectrum of the SBA-15-MPS sample. The band at 2584 cm^{-1} in the spectrum of the MPS-modified sample (Figure 3b) is assigned to the S−H stretching vibrations.

Figure 4 shows the ^{13}C NMR spectra of the SBA-15-MPS sample. The peak at 9.3 ppm was attributed to the C^1 carbon

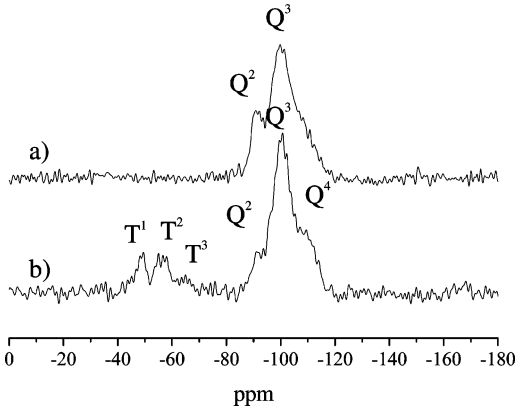

Figure 5. ^{29}Si NMR spectra of the (a) calcined and (b) thiol-modified SBA materials.

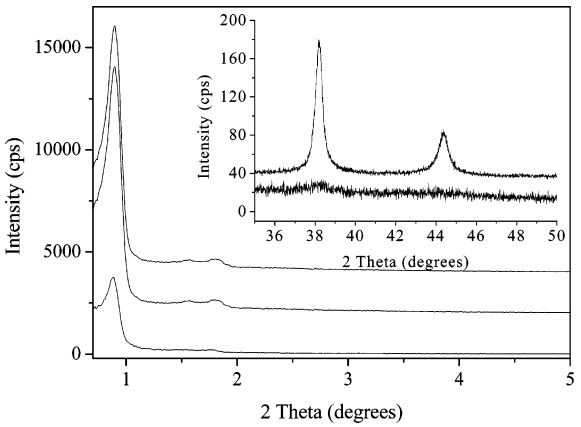

Figure 6. Small-angle XRD patterns of the (a) SBA-15-MPS, (b) SBA-15-MPS-Au1, and (c) SBA-15-MPS-Au1-red samples (inset: wide-angle XRD patterns).

atoms of the methylene groups that are directly bonded to the Si atoms. The signals at about 27.2 and 49.1 ppm were assigned to the other two carbon atoms (C^2 and C^3) from the propyl chain as shown in Figure 4. The assignments correspond to other results shown in the literature.[29,30]

The nature of the molecular functionalities and the chemical bonding to the silica surface of the mesoporous material can by studied by solid-state ^{29}Si NMR. In the ^{29}Si NMR spectrum of the calcined SBA-15 material two distinct chemical shifts were recorded at −90.8 and −99.8 ppm that are attributed to silicon in the siloxane binding environment with geminal silanol groups [$(SiO)_2Si-(OH)_2$] (Q^2 silicon atoms) and to isolated silanol groups [$(SiO)_3Si-(OH)$] (Q^3 silicon atoms). Only a shoulder of low intensity was detected at −110 ppm, which is due to silicon atoms in a siloxane environment with no silanol groups [$(SiO)_4Si$] (Q^4 silicon atoms) (Figure 5a).[16,29,30] The chemical shifts at about −100 and −109.7 ppm are assigned to the Q^3 and Q^4 silicon atoms in the spectrum of the SBA-15-MPS sample (Figure 5b). In comparison to the ^{29}Si NMR spectrum of the calcined SBA-15 material (Figure 5a), the appearance of fully cross-linked Si atoms (Q^4) and the considerable decrease of the Q^2 species in the spectrum of the SBA-15-MPS material is indicative for the increased siloxane condensation via reaction of the organosilane with the surface silanols. The appearance of the residual Q^2 species in the spectrum of the MPS-modified sample suggests the existence of Si bearing OH groups that did not participate in the cross-linking of the organosilane molecules. Signals from the T^n silicon atoms (silicon atoms in the organosilane molecules) were also observed in the spectrum of the SBA-15-MPS sample. Figure 5b shows signals at about 49.1, 56.7, and 65.5 ppm that are attributed to the T^1 (silicon atoms that are bound to two hydroxyl, one organic residue, and one siloxane bridge [(SiO)-$Si-(OH)_2R$]), T^2 (silicon atoms that are bound to one hydroxyl and one organic residue, and form two siloxane bridges [$(SiO)_2Si-(OH)R$]), and T^3 (silicon atoms that form three siloxane bonds [$(SiO)_3Si-R$]).[16,29,30] The predominant appearance of the T^1 and T^2 silicon atoms suggests the formation of a sparsely covered mesoporous surface with mostly isolated MPS molecules and the absence of large fully cross-linked aggregates of thiol-silane itself.[29,30] The relative integrated intensities of the NMR signals of the organosiloxanes (T^n) and siloxane species (Q^n) can be employed to estimate the incorporated amount of functional groups.[31] The percentage of the reacted surface silanol groups with organosilane molecules can be estimated by taking into account the ratio of the integrated intensities of the NMR signals for T^n ($= T^1 + T^2 + T^3$) and Q^n ($= Q^2 + Q^3 + Q^4$) silicon atoms. The calculated T^n/Q^n ratio from the ^{29}Si NMR spectrum shown in Figure 5b is 0.23. The calculated MPS loading from the TGA (see before) is lower than that estimated from the ^{29}Si NMR data. It should be noted that the relative peak intensities in the ^{29}Si NMR spectra are not strictly quantifiable due to possible differences in the relaxation behavior.

3.2. Assembly of the Au Precursors and Gold Electroless Reduction. Figure 6 shows small-angle and wide-angle (inset in Figure 6) XRD patterns of the MPS-modified SBA-15 sample subjected to the Au1 colloid in toluene followed by electroless reduction. The mesophase structure is preserved at every modification step as seen from the small-angle XRD patterns. The decrease in the intensity of the first-order reflection can be attributed to the decreased scattering contrast due to the pore filling effect.[16] The wide-angle XRD patterns show that after the co-assembly of the Au nanoparticles (∼5 nm in diameter) a very low intensity, broad diffraction peak at about 38.1° 2θ is recorded that can be assigned to (111) reflection of the crystalline Au. The crystalline size of the Au nanostructures assembled from the Au1 colloidal suspension, calculated from the Scherrer equation, is 5.7 nm (Table 1). After the electroless reduction, the wide-angle XRD pattern shows distinct (111) and (200) reflections of crystalline Au that correspond to crystalline domains with sizes of about 20 nm.

The second type of gold precursors (the Au2 solution), containing $[AuCl_4]^-$ ions complexed to TOAB molecules, were assembled on the SBA-15-MPS mesoporous surface, followed by electroless reduction with the same plating bath. The small-angle XRD patterns, taken after these modification steps, show that the mesophase structure is preserved (Figure 7). In the wide-angle XRD patterns of the SBA-15-MPS-Au2 sample no crystalline Au was detected. After the electroless reduction, the wide-angle XRD pattern shows the appearance of crystalline Au with an average size of the crystalline domains determined from the Scherrer equation of about 22 nm.

The N_2-adsorption measurements were undertaken to further confirm the pore-filling effect due to the incorporation of the Au nanostructures in the mesoporous host (Figure 8). Generally, the shape of the isotherm is preserved after every modification step in agreement with the preserved mesostructural order of the samples. Hysteresis loops with similar shapes were obtained for all samples showing the absence of pore clogging. Most importantly, the calculated surface area (S_{BET}), the mean pore size diameter (D_{BJH}), and the total pore volume (V_t) show a continuous decrease from the values obtained for the SBA-15-MPS sample to the samples subjected to electroless reduction

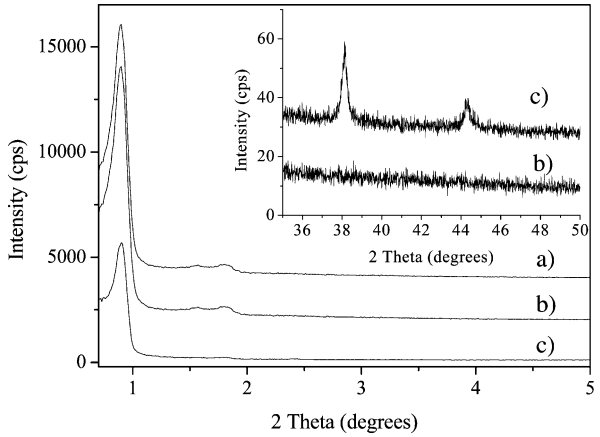

Figure 7. Small-angle XRD patterns of the (a) SBA-15-MPS, (b) SBA-15-MPS-Au2, and (c) SBA-15-MPS-Au2-red samples (inset: wide-angle XRD patterns).

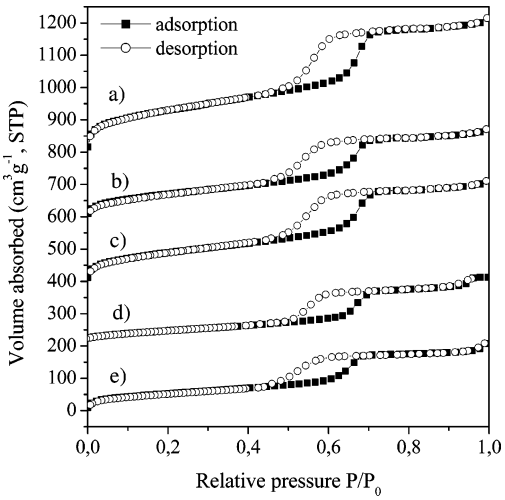

Figure 8. N_2 adsorption isotherms of the (a) SBA-15-MPS, (b) SBA-15-MPS-Au1, (c) SBA-15-MPS-Au2, (d) SBA-15-MPS-Au1-red, and (e) SBA-15-MPS-Au2-red samples (the isotherms are offset with 200 $cm^3\ g^{-1}$).

(Table 1). The substantial difference between the accessible pore volume of the mesoporous support and the calculated volume occupied by Au nanostructures after gold loading determined by EDX (see below) does not give clear verification for the templating role of the SBA-15 host. A direct proof of the templating role of the SBA-15 host material in the growth of the Au nanostructures can be obtained by applying transmission electron microscopy.

Panels a and b in Figure 9 show the TEM images of the SBA-15-MPS-Au1 and SBA-15-MPS-Au1-red samples. After assembly of the Au1 colloid the mesophase structure is preserved (in agreement with the XRD results) and Au nanoparticles, 4−6 nm in diameter (shown with arrows in the image), are visible on the mesophase surface (may be only on the outer surface). The usually isolated Au nanoparticles with diameters corresponding to those observed in the initial Au1 colloid were observed. In some cases, Au aggregates were also seen, which could be responsible for the increased particle size determined with the Scherrer equation. The number density of the Au nanoparticles onto the mesoporous host is relatively low. After the electroless reduction (Figure 9b), the TEM images show formation of bigger Au nanoparticles with diameters of more than 30 nm, in correspondence with the XRD results. It appears that the growth of the Au nanoparticles is not templated by the

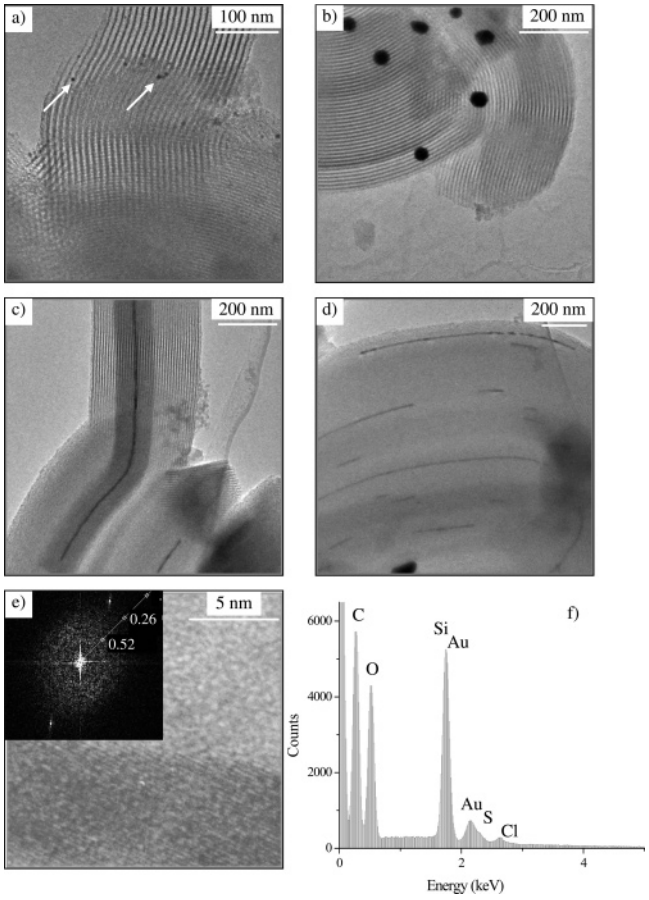

Figure 9. TEM images of the (a) SBA-15-MPS-Au1 and (b) SBA-15-MPS-Au1-red and SBA-15-MPS-Au2-red samples and (c and d) two different magnifications, (e) HR-TEM image of a single-crystalline Au domain, and (f) EDX analysis of the SBA-15-MPS-Au2-red sample (inset in panel e: power spectrum calculated from the corresponding image).

mesophase structure. The particles are randomly distributed over the whole outer surface of the mesoporous material (Figure 9b). The density of the Au nanoparticles is similar to that before the electroless reduction suggesting that the 5 nm Au nanoparticles served as nucleation centers for the subsequent growth of bigger Au nanoparticles. The Au loading before and after electroless reduction was determined with EDX (data not shown). The Au loading in the SBA-15-MPS-Au1 was below the detection limit of the EDX at the experimental conditions used in this study. After the electroless reduction, the signals of the Au atoms were detected with an Au/Si atom ratio of 0.07. The estimated gold loading after the electroless reduction is about 2.1 wt %.

The TEM results for the Au2 precursors assembled onto the SBA-15-MPS surface and subjected to electroless reduction show completely different Au nanostructures (Figure 9c−e). For the SBA-15-MPS-Au2 sample no crystalline Au nanostructures can be observed at the used magnification in agreement with the XRD results. After the electroless reduction, Au nanowires with uniform diameter of about 5 nm corresponding to the pore size of the host material were observed. Usually, the Au nanowires show different lengths in the range of 100−1000 nm, some of them reaching more than 3 μm (Figure 9d). Very few other Au nanostructures, such as Au spheres or agglomerates with dimensions of about 10−20 nm in diameter, were observed. These are not templated by the host matrix and might be the reason for the higher average crystalline domain size determined from the Scherrer equation (Table 1). Figure 9c clearly shows

that the growth of the Au nanowires is templated by the channel structure of the SBA-15 material. Additionally, TEM images were taken of isolated Au nanowires after dissolving the silica support in 8% HF (data not shown). The Au nanowires appeared isolated in contrast to the connected Pt nanowires prepared in SBA-15 material by wet chemical impregnation.[32] In our case, the unconnected Au nanowires suggest that the additional microporosity of the SBA-15 walls, responsible for bundling the Pt nanowires, was masked during the silane modification. The number density of the Au nanowires is smaller than that observed on the ammonium-modified MCM-41 material prepared by H_2 reduction where Au particles on the outer surface were also detected.[16] This can be attributed to sparsely covered mesoporous surface with thiol functionalities and restricted diffusion as the first Au segments are formed inside the mesoporous channel system. The HR-TEM images of the Au nanowires templated in the SBA-15 support reveal that each nanowire consists of uniform, single-crystalline Au segments (Figure 9e). The {111} set of lattice planes of the Au nanowires were observed with a *d* spacing of about 0.24 nm calculated from the corresponding power spectrum (inset in Figure 9e). Usually, the length of such parts exceeds several tens of nanometers. The Au nanowires prepared inside the nanosized channels of the SBA-15 material show extremely high aspect ratios with large single-crystalline Au domains. The loading with Au nanowires was estimated with the EDX analysis (Figure 9f). Before electroless reduction no Au was detected (close to the detection limit of the EDX); the signals of the Si and S atoms appear with an S/Si atom ratio of 0.05. After electroless reduction the Au/Si atom ratio was measured to be 0.05 corresponding to about 1.5 wt % Au loading. This is less than that observed for the SBA-15-MPS-Au1-red sample.

Comparing the results from the first synthetic approach (with the Au1 colloid as a precursor for the electroless reduction) and the second synthetic approach (with the Au2 solution as a precursor for the electroless reduction) it is clear that the dimensions and the nature of the Au precursors are critical for the subsequent electroless reduction process. In the first case, the 3−5 nm Au nanoparticles were assembled preferentially on the outer surface or pore entrance of the MPS-modified mesoporous material and thus may totally block the pores of SBA-15 resulting in decreased accessible pore volume determined by N_2 adsorption. These Au seeds gave rise to the growth of 20−60 nm Au particles where no templating role of the mesoporous support was observed. It can be argued that the diffusion of these 3−5 nm Au precursors into the channel system of the SBA-15 material is hindered because of the almost equal pore size of the host matrix. Even if some of the Au1 nanoparticles gain access to the channel system of the SBA-15 material, the necessary diffusion of the $[AuCl_4]^-$ ions during the electroless reduction would be considerably restricted. Thus, the nucleation sites for the electroless reduction are preferentially formed on the outer surface of the mesoporous material and resulted in unrestricted growth of bigger Au particles. In contrast, during the assembly of the Au2 solution onto the MPS-modified SBA-15 material, a very thin layer of Au precursors ($[AuCl_4]^-$ ions complexed to TOAB molecules) is formed on the mesoporous surface that allows easy diffusion of the $[AuCl_4]^-$ and the reducing agent into the channel system during the subsequent electroless reduction process. Thus, high aspect ratios of Au nanowires are formed templated by the SBA-15 channel system and isolated from each other through rigid silica walls. In addition, the extremely thiophilic nature of Au is responsible for the chemisorption of the Au precursors (FT-Raman spectra of the SBA-15-MPS samples showed disappearance of the S−H stretching vibrations upon modification with Au2 precursors) onto the polymeric adhesive layers having pedant thiol groups and covalently bonded to the mesoporous silica surface. Blank experiments with unmodified SBA-15 support showed hardly any adsorption of Au precursors and no activity in subsequent electroless reduction processes. The lower number density and nonuniform distribution of the Au nanowires prepared from Au2 precursors may be attributed to the sparsely covered mesoporous surface with thiol functionalities.

The similarity of the XRD and the N_2-adsorption results for both synthetic approaches shows that often in inclusion chemistry such results must be interpreted with great care. For example, the decreased intensity of the mesoporous Bragg peaks is in most cases explained by the decreased scattering contrast between the pores and the walls due to the pore filling effect, but another reasonable explanation could be the decreased structural order in the mesoporous material. It seems that the TEM measurements are essential for such investigations although in many cases TEM is considered to be a local probe measurement.

4. Conclusions

A new synthetic method for the preparation of Au nanostructures in mesoporous SBA-15 hosts based on the electroless reduction of Au was developed. Two different approaches for the introduction of the seed species for the electroless reduction were investigated. It is shown that the $[AuCl_4]^-$ ions complexed to the TOAB molecules, assembled on the thiol-modified mesoporous surface of the SBA-15 material are suitable precursors for the subsequent electroless reduction. The resulting structures show micrometer long Au nanowires with uniform diameters of about 5 nm and large single-crystalline domains. The experimental results clearly show that the growth of the Au nanowires is templated by the channel structure of the SBA-15 material.

Acknowledgment. The authors thank the SFB 486-B-8 project for financial support.

References and Notes

(1) Xia, Y.; Yang, P.; Sun, Y.; Wu, Y.; Mayers B.; Gates B.; Yin, Y.; Kim F.; Yan, H. *Adv. Mater.* **2003**, *15*, 353.
(2) Wirtz, M.; Martin, C. R. *Adv. Mater.* **2003**, *15*, 455.
(3) Wang, Z. L. *Adv. Mater.* **2003**, *15*, 1497
(4) Schwerdtfeger, P. *Angew. Chem., Int. Ed.* **2003**, *42*, 1892.
(5) Wynwa, D.; Beyer, N.; Scmid, G. *Nano Lett.* **2002**, *2*, 419.
(6) Foss, C. A.; Tierney, M. J.; Martin, C. R. *J. Phys. Chem.*, **1992**, *96*, 9001.
(7) Whitney, T. M.; Jiang, J. S.; Searson, P. C.; Chien, C. L. *Science* **1993**, *261*, 1316.
(8) Preston, C. K.; Moskovits, M. *J. Phys. Chem.* **1993**, *97*, 8495.
(9) Schmid, G. *J. Mater. Chem.* **2002**, *12*, 1231.
(10) Martin, C. R. *Chem. Mater.* **1996**, *8*, 1739.
(11) Han, Y.-J.; Kim, J. M.; Stucky, G. D. *Chem. Mater.* **2000**, *12*, 2068.
(12) Kohn, R.; Froeba, M. *Catal. Today* **2001**, *68*, 227.
(13) Mehnert, C. P.; Weaver, D. W.; Ying, J. Y. *J. Am. Chem. Soc.* **1998**, *120*, 12289.
(14) Kang, H.; Jun, Y. W.; Park, J. I.; Lee, K.-B.; Cheon, J. *Chem Mater.* **2000**, *12*, 3530.
(15) Lee, K.-B.; Lee, S.-M.; Cheon, J. *Adv. Mater.* **2001**, *13*, 517.
(16) Yang, C.; Shue, H.; Chao, K. *Adv. Funct. Mater.* **2002**, *12*, 143.
(17) Yang, C.; Liu, P.; Ho, Y.; Chiu, C.; Chao, K. *Chem. Mater.* **2003**, *15*, 275.
(18) Guari, Y.; Thieuleux, C.; Mehdi, A.; Reye, C.; Corriu, R. J. P.; Gomez-Gallardo, S.; Philippot, K.; Chaudret, B.; Dutartre, R. *Chem. Commun.* **2001**, 1374.
(19) Guari, Y.; Thieuleux, C.; Mehdi, A.; Reye, C.; Corriu, R. J. P.; Gomez-Gallardo, S.; Philippot, K.; Chaudret, B. *Chem. Mater.* **2003**, *15*, 2017.
(20) Zhu, H.; Lee, B.; Dai, S.; Overbury, S. H. *Langmuir* **2003**, *19*, 3974.

(21) Mukherjee, P.; Sastry, M.; Kumar, R. *Phys. Chem. Commun.* **2000**, 4.
(22) Zhang, Z.; Dai, S.; Blom, D. A.; Shen, J. *Chem. Mater.* **2002**, *14*, 965.
(23) Spector, M. S.; Price, R. R.; Schnur, J. M. *Adv. Mater.* **1999**, *11*, 337.
(24) Braun, E.; Eichen, Y.; Sivan, U.; Ben-Yoseph, G. *Nature* **1998**, *391*, 775.
(25) Harnack, O.; Ford, W. E.; Yasuda, A.; Wessels, J. M. *Nano Lett.* **2002**, *2*, 919.
(26) Zhao, D.; Sun, J.; Li, Q.; Stucky, G. D. *Chem. Mater.* **2000**, *12*, 275.
(27) Brust, M.; Bethell, D.; Kiely, C. J.; Schiffrin, D. J. *Langmuir* **1998**, *14*, 5425.
(28) Menzel, H.; Mowery, M. D.; Cai, M.; Evans, C. E. *Adv. Mater.* **1999**, *11*, 131.
(29) Feng, X.; Fryxell, G. E.; Wang, L.-Q.; Kim, A. Y.; Liu, J.; Kenner, K. M. *Science* **1997**, *276*, 923.
(30) Liu, A. M.; Hidajat, K.; Kawi, S.; Zhao, D. Y. *Chem. Commun.* **2000**, 1145.
(31) Yoshitake, H.; Yokoi, T.; Tatsumi, T. *Chem. Mater.* **2002**, *14*, 4603.
(32) Liu, Z.; Terasaki, O.; Ohsuna, T.; Hiraga, K.; Shin, H. J.; Ryoo, R. *ChemPhysChem* **2001**, *4*, 229.